



Research article

Repurposing of known drugs from multiple libraries to identify novel and potential selective inhibitors of HDAC6 via *in silico* approach and molecular modeling

Naz Mina Mert, Buse Erdogan, Kemal Yelekçi*

Department of Molecular Biology and Genetics, Faculty of Engineering and Natural Sciences, Kadir Has University, 34083, Cibali, Istanbul, Turkey

ARTICLE INFO

Keywords:

HDAC6
Cancer
In silico screening
Docking
M.D. simulation
HDAC6 selective inhibitors

ABSTRACT

Histone deacetylase 6 (HDAC6, Class IIb) is a promising target for anticancer drugs. So far, few nonselective HDAC inhibitors have received regulatory approval as anticancer agents. However, they are associated with cell toxicity. Thus, isoform-selective inhibitors may be desirable. Here, we conducted structure-based virtual screening of multiple libraries containing a total of 2,250,135 compounds against HDAC6. The top hits with good docking scores and potential selectivity over HDAC10 (Class IIb) were submitted to 100 ns molecular dynamics simulation to monitor their dynamic behaviors and stability in the binding pockets of these enzymes. Furthermore, the drug-likeness and ADMET properties of these hits were estimated computationally. Four diverse compounds from different sources, including NCI and ZINC databases (BDH33926500, CID667061, Cromolyn, and ZINC000103531486), show potential selectivity for HDAC6.

1. Introduction

Epigenetic mechanisms are crucial to maintaining regular growth, development, and gene expression in the human body. Therefore, epigenetic modifications that lead to changes in gene expression have been determined to be one of the most important causes of cancer development and progression [1]. Targeting these epigenetic alterations is one of the crucial strategies for cancer treatment. Among several posttranslational modifications, the deacetylation of histone proteins is the most exploited strategy [2]. Histone deacetylases (HDACs) display a crucial role in various cellular and mechanistic pathways [3], catalyzing the deacetylation processes of the N-terminal lysine residues of the histone and nonhistone proteins regulating the gene expression [4]. Targeting HDACs in cancer treatment has become a widely used strategy [5].

Up to now, eighteen mammalian HDAC isoforms are grouped into four classes, namely class I HDACs (1, 2, 3, and 8), class IIa HDACs (5, 7, 9), and IIb (6 and 10), class III HDACs (Sirtuins), and class IV (HDAC11) [6]. Class IIb has two isoforms: HDAC6 and HDAC10. These isozymes are primarily localized in the cytoplasm of the mammalian cells, so they act on the nonhistone proteins [7]. HDAC6 is the largest HDAC isoform with 1215 amino acids identified in humans, harboring two independent catalytic domains. On the other hand, HDAC10 has only one functional catalytic domain [8].

HDAC6 isoform plays a crucial role in the deacetylation of the α -tubulin in microtubules, controlling the cell motility and microtubule stability [9]. Additionally, HDAC6 is implicated with neurodegenerative diseases such as Parkinson's disease and

* Corresponding author.

E-mail address: yelekci@khas.edu.tr (K. Yelekçi).

<https://doi.org/10.1016/j.heliyon.2024.e35020>

Received 26 March 2024; Received in revised form 19 July 2024; Accepted 22 July 2024

Available online 23 July 2024

2405-8440/© 2024 The Authors. Published by Elsevier Ltd. This is an open access article under the CC BY-NC license (<http://creativecommons.org/licenses/by-nc/4.0/>).

Alzheimer's disease [10]. HDAC6 is a potential drug target due to its involvement in various cellular processes such as tumorigenesis, apoptosis, and growth of various malignancies Cosenza & Pozzi, 2018.

Inhibition of HDAC6 is associated with less toxicity than other HDACs [11]. HDAC inhibitors comprise three specific parts: a zinc-binding group (ZBG), a linker, and a capping group. The ZBG forms a strong complex with zinc cation within the enzyme active site. The linker group spans the entire pocket area and connects to the cap group, serving as a surface recognition group [12]. So far, inhibitors such as vorinostat (suberoyl hydroxamic acid (SAHA)) (Grant et al., 2007), belinostat [13], romidepsin [14] and panobinostat [15] have been approved by The Food and Drug Administration for the treatment of hematological cancers. A few class-selective inhibitors are in clinical trials for solid and non-solid malignancies. These drugs are considered pan-HDAC inhibitors because they target multiple isoforms, consequently associated with cell toxicities causing side effects such as diarrhea, vomiting, and fatigue [16]. On the other hand, isoform-selective HDAC inhibitors show less side effects [17]. Previously, we applied structure-based and ligand-based virtual screenings [12] to identify potential selective inhibitors of HDAC6 and ran shorter (under 50 ns) M.D. simulations to examine ligand binding mode stability.

In the continuous search for HDAC6-selective inhibitors, we conducted an elaborated structure-based virtual screening of multiple libraries containing 2,250,135 compounds. The top hits were subjected to ADMET prediction analysis and submitted to a 100 ns M.D. simulation to examine the stability of the ligand-binding mode. Four compounds from different databases show potential selectivity for HDAC6.

2. Materials and methods

2.1. Protein setup

The X-ray crystallographic structure of human HDAC6 (5EDU) catalytic domain two complexed with Trichostatin A (TSN) inhibitor

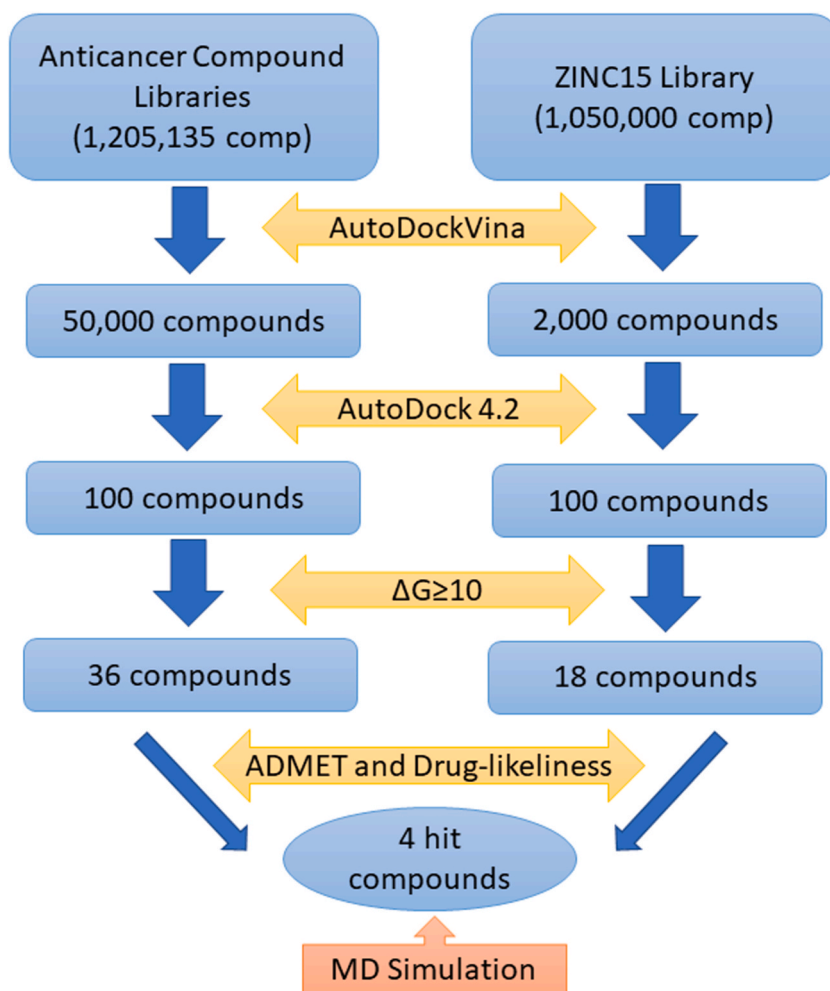


Fig. 1. Virtual screening workflow for identifying selective and potent lead compounds for HDAC6.

with a resolution of 2.79 Å was retrieved from the PDB website (<https://www.rcsb.org/>) [18]. Water molecules, native ligands, and salt ions were removed from the HDAC6 crystal structure, hydrogen atoms were added using BIOVIA DS 4.5 [19], and the structure was subjected to short minimization to correct the bond order and distance. Then, the native ligand (TSN) was docked into the HDAC6 active site to check the RMSD value for structure validation. RMSD was 1.52 Å, an acceptable value for the reference ligand. The protein was prepared with the protocol at an optimum pH of 7.4 "Prepare Protein" in BIOVIA DS 4.5. The isozyme HDAC10 was prepared for docking as described in our previous paper [12].

2.2. Ligand setup

A library of 1,205,135 anticancer agents was built from multiple databases, including the National Cancer Institute (NCI), Asinex, SelleckChem, Hypha, Cambridge, DrugCentral, Enzo, Molport, Art-Chem, NIH, and the ZINC15 druglike library containing 1,050,000 compounds (<https://zinc15.docking.org/>) [20]. The ZINC15 dataset contains molecular weights ranging from 200 to 500 druglike compounds with specific LogP values. The compound libraries were further prepared using the "Prepare Ligands" protocol by BIOVIA DS 4.5 at pH 7.4, protonated at this pH value, 3D geometries were optimized, and files were saved in SDF file format.

2.3. Structure-based virtual screening

Structure-based virtual screening (SBVS) is a widely used and robust *in silico* method for drug screening. In this study, AutoDock

Table 1
ADMET properties of 36 hit compounds from cancer libraries performing AdmetSAR and SwissADME servers.

	Compound Name	MlogP ^a	logS ^b	MW ^c	HA ^d	HD ^e	TPSA ^f	Caco-2 perm. ^g	HIA + ^h
1	BDE 30366547	1.23	-2.4295	481.64	6	3	105.31	0.1402	0.9935
2	Florantyrone	3.45	-4.2153	302.32	3	1	54.37	0.9325	0.9930
3	Tiagabine	3.32	-2.1831	375.55	3	1	97.02	1.0191	0.9603
4	BDH 33926500	1.02	-3.4187	464.51	7	2	116.09	0.3738	0.6043
5	LEG 08800372	1.59	-3.0930	434.49	4	3	109.68	0.1776	0.9593
6	BDE 30366622	1.37	-2.6862	426.56	5	3	102.07	0.1989	0.9747
7	compound 50032	2.93	-3.4890	383.4	3	3	98.8	0.7462	0.9950
8	CID 667061	2.1	-4.0150	485.53	5	1	104.09	0.9196	0.9811
9	Cromolyn	-1.11	-2.9089	466.35	11	1	179.37	0.0720	0.7708
10	CID 2891529	4.76	-3.8595	447.48	4	1	74.68	1.0680	0.9904
11	CID 2892576	3.32	-3.9607	427.49	4	2	75.63	0.6695	0.9556
12	CID 2927618	3.95	-3.6806	397.47	3	2	66.4	1.2458	0.9935
13	CID 1607669	1.69	-3.3978	491.56	7	4	155.68	0.3940	0.9749
14	CID 1245041	1.94	-3.4653	358.34	5	1	84.58	0.9443	1
15	CID 87331676	2.03	-4.1283	486.61	4	3	99.87	0.6314	1
16	CID 2517760	2.38	-4.1668	265.26	4	1	63.33	1.3515	1
17	compound 1784	3.88	-4.4985	400.4	5	0	86.74	1.1891	0.9479
18	CID 6059452	1.28	-3.0900	444.44	5	3	120.74	0.8091	0.9826
19	CID 1347479	2.53	-3.7711	357.42	4	1	83.06	0.7684	1
20	CID 1325129	1.39	-3.5610	361.37	6	2	110.31	0.4639	0.9941
21	CID 6236333	4.11	-3.8890	415.27	4	1	72.19	0.7898	0.9695
22	CID 16317746	1.84	-3.5795	469.55	5	1	112.24	0.4364	0.9617
23	CID 24789568	3.07	-3.6420	479.48	8	1	138.11	0.6437	0.9947
24	CID 885323	2.3	-3.6924	343.4	4	1	83.06	0.7179	1
25	ZINC 257329731	0.95	-3.0728	474.64	6	2	99.34	0.6080	0.7220
26	BDE 30671222	2.21	-2.3968	480.65	5	2	93.28	0.2446	0.9586
27	BDE 30366549	1.23	-2.3618	481.64	6	3	105.31	0.1762	0.9919
28	BDC 22516221	1.98	-3.3381	446.58	4	1	90.03	0.7164	0.9897
29	Hypha223	2.03	-4.1283	486.61	4	3	99.87	0.6314	0.9629
30	Hypha417	3.34	-3.0082	398.58	4	1	33.73	1.0838	0.9873
31	compound 903	2.68	-3.7361	438.43	6	2	105.04	0.2720	0.9753
32	CID 13789	0.33	-2.5201	343.38	5	1	75.02	0.5231	0.8268
33	CID 2135742	2.63	-3.3193	384.43	4	2	93.12	0.9074	0.9148
34	CID 2867309	2.65	-3.6480	427.37	6	2	124.09	1.0121	1
35	CID 1931770	2.95	-4.3208	458.85	6	2	105.04	0.4219	0.9642
36	CID 5429429	3.81	-3.7956	496.49	6	2	95.94	0.8526	0.9271

^a Moriguchi model of octanol-water partition coefficient, LogP.

^b Aqueous Solubility, LogS.

^c Molecular weight in Da.

^d Total number of H-bond acceptors, N and O.

^e Total number of H-bond donors, NH and OH.

^f Topological polar surface area in Å².

^g Caco-2 Permeability in cm/s.

^h Human intestinal absorption.

Vina [21] (<http://vina.scripps.edu/>) was used efficiently in the screening process. The Lamarckian genetic algorithm was used to generate docking input files. Grid box parameters were set to $X = 17.1$, $Y = -44.5$, and $Z = 102.7 \text{ \AA}$, covering the active site, and grid box dimensions were set to $55 \times 55 \times 55 \text{ \AA}$ with the spacing of 0.375 \AA . The x,y, and z coordinates were determined based on the known reference ligand Trichostatin A (TSN) as a native inhibitor for HDAC6 for virtual screening. Ten runs were allowed for each ligand with medium (2,500,000) evaluations and the Lamarckian genetic algorithm. The same workflow was applied to the compounds, starting screening with AutoDockVina, and the top 50,000 ligands from anticancer compound libraries and 2000 ligands from the ZINC15 library showing the best affinities were selected and filtered based on the Lipinski rule of five. Then, the top 100 compounds from both libraries showing good binding affinity passed the criteria for further docking using AutoDock 4.2 into HDAC6 and cross-docked with HDAC10 to search for potential selective inhibitors of HDAC6. A hundred compounds satisfied the criterion of $\Delta G \geq 10$ against HDAC6, out of which 18 compounds from the ZINC15 database and 36 compounds from cancer-like compound libraries (FDA-Approved, NIH, Asinex, and NCI) showed good drug-likeness and ADMET properties. Finally, four hit compounds showed potential selectivity for HDAC6 over HDAC10 (Fig. 1).

2.4. ADMET prediction

ADMET properties of novel and potential 36 compounds from the anticancer and 18 hits from ZINC libraries were predicted by *in silico* techniques using the SwissADME server (<http://www.swissadme.ch/>) and AdmetSAR server (<http://lmmd.ecust.edu.cn/admetSar1>) shown in Tables 1 and 2.

All 36 compounds from libraries containing anticancer compounds and 18 target compounds from the ZINC library satisfy the “Rule of 5” since the druglike molecules should obey the rule with no more than one violation [22]. The prediction of the caco-2 permeability, TPSA, LogS, HIA, and MlogP values of all the selected hit compounds for HDAC6 were within the normal range except for Cromolyn, which had a slightly higher TPSA value. The best four compounds (3 from anticancer compound libraries and one from the ZINC library) showing the most significant binding affinity and enzyme selectivity were selected. Finally, a molecular dynamics simulation was performed for these top compounds with HDAC6.

2.5. Molecular dynamics simulation

Molecular dynamics simulations (M.D.s) predict each atom’s spatial position and motion in a protein at every point in time by interatomic interactions; M.D. simulations were carried out on the complexes of HDAC6 with TSN, BDH33926500, CID667061, Cromolyn, and ZINC000103531486. All MD simulations were performed using the Nanoscale Molecular Dynamics (NAMD) software [23]. The systems were prepared using the CHARMM-GUI web server (<https://www.charmm-gui.org/>) [24] on which NAMD input files were generated according to CHARMM36 m force field and ligands were parameterized via CHARMM General Force Field (CGenFF) server (<https://cgenff.umaryland.edu/>). The systems were solvated with the TIP3 water module and neutralized by adding

Table 2

Drug-likeness and ADMET properties of 18 hit compounds from the ZINC library using AdmetSAR and SwissADME servers.

	Compound Name	MlogP ^a	logS ^b	MW ^c	HA ^d	HD ^e	TPSA ^f	Caco-2 perm. ^g	HIA + ^h
1	ZINC000013655575	2.86	-3.8365	449.85	7	2	126.91	0.325	0.8426
2	ZINC000064979644	2.62	-4.1848	431.94	5	0	75.03	1.008	1
3	ZINC000013655575	2.86	-3.8746	449.85	7	2	126.91	0.3401	0.9646
4	ZINC000019712236	2.48	-3.3883	447.53	5	3	109	1.1262	1
5	ZINC000012882053	2.06	-3.7089	428.52	5	1	124.19	0.2658	0.9915
6	ZINC000101969184	-0.13	-1.998	445.58	4	1	68.35	0.5647	0.9308
7	ZINC000245232199	2.3	-3.7814	435.47	5	1	112.3	0.713	1
8	ZINC000245284480	-0.13	-1.998	445.58	4	1	68.35	0.5647	0.9308
9	ZINC000023075384	2.6	-3.4491	437.47	7	1	126.14	0.3791	1
10	ZINC000103531486	3.68	-3.8057	491.51	6	3	134.54	0.3489	0.9226
11	ZINC000261361753	2.83	-3.892	476.32	5	3	134.54	0.4175	0.8642
12	ZINC000001001148	2.06	-3.4029	480.47	5	1	119.3	0.5576	0.9973
13	ZINC000014745209	-0.43	-3.5277	470.58	3	1	58.2	1.0745	0.9931
14	ZINC000257288501	1.71	-3.061	453.48	7	2	105.53	0.6002	0.7519
15	ZINC000257333130	1.71	-3.061	453.48	7	2	105.53	0.6002	0.7519
16	ZINC000103531486	2.73	-3.4418	494.5	5	1	115.54	1.1473	1
17	ZINC000040156325	3	-3.7806	455.91	5	3	120.53	-0.1317	0.9901
18	ZINC000257209181	1.92	-3.017	467.51	7	1	94.53	0.9526	0.7153

^a Moriguchi model of octanol-water partition coefficient, LogP.

^b Aqueous Solubility, LogS.

^c Molecular weight in Da.

^d Total number of H-bond acceptors, N and O.

^e Total number of H-bond donors, NH and OH.

^f Topological polar surface area in \AA^2 .

^g Caco-2 Permeability in cm/s.

^h Human intestinal absorption.

the K^+ and Cl^- ions (KCl) with a concentration of 0.15 M by the distance (systematic) method. First, energy minimization was done for 10,000 steps (20ps), and then equilibration for two ns was done at a constant number of atoms, volume, and temperature (NVT) ensembles. Finally, a 100 ns unrestrained production simulation was conducted at a constant number of atoms, pressure, and temperature (NPT) ensemble. During the unrestrained production run, the time step was set to 2 fs, and the frame was saved every 5000 steps. The stability of the enzyme-ligand complex binding mode was assessed by computing root-mean-square fluctuation (RMSF), root-mean-square deviation (RMSD), and the radius of gyration (Rg) profiles for each system using Visual Molecular Dynamics (VMD) [23].

3. Results and discussion

3.1. Molecular docking scores

The estimated docking scores of the best potential selective hits are given in Table 3. Out of the 100 compounds docked into the active site of both HDAC6 and HDAC10, four compounds (Compounds BDH33926500, CID667061, Cromolyn, and ZINC000103531486) from diverse libraries demonstrate the highest potency and selectivity for HDAC6 over HDAC10. Compounds with various structures have been proposed as HDAC6-selective and potent inhibitors.

The comparison of the inhibition constant values indicated that BDH33926500 150.89-fold, CID667061 48.76-fold, Cromolyn shows 1055.74-fold and ZINC000103531486 1019.5-fold selective over HDAC10 ($K_{iHDAC10}/K_{iHDAC6}$). Among all the other hit compounds, ZINC000103531486, with the highest binding energy of -14.21 kcal/mol and high selectivity values, seems to be the best potential drug candidate.

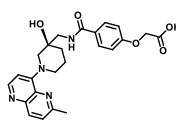
3.2. Protein-ligand interaction

BDH33926500, CID667061, and Cromolyn compounds were docked into the HDAC6 active site. They all form various interactions with the critical amino acid side chain in the catalytic channel, including salt bridges, van der Waals interactions, hydrogen bonds, π -cation, π -sulfur interaction, alkyl, π -alkyl, amide- π stacked interactions, attractive charge, π - π stacked, π - π T-shaped and π -sigma. Fig. 2 shows the interactions between HDAC6 and Trichostatin (TSN) in 3D (A) and 2D (B). The types of nonbonded interactions are indicated in the 2D scheme in respective colors. Hydroxamic acid moiety interacts with Zn^{2+} ions correctly, agreeing with the crystal structure position. Both the position of Trichostatin and the interacting residues in the active site of the HDAC6 satisfy the validation requirement, which means the enzyme is suitable for modeling studies. Compound BDH33926500 interacts with the catalytic channel Zn^{2+} atom as a metal-acceptor through their carboxyl groups by electrostatic attraction. Also, the compound interacts with the catalytically essential residues HIS610, HIS 611, and TYR 782 via a conventional hydrogen bond. BDH33926500 forms π - π stacked interactions with the PHE 620 and PHE 680 residues (Fig. 3). Similarly, CID667061 forms π - π stacked interactions with PHE 620, HIS 651 and PHE 680 and additional π - π stacked interaction with the residue HIS 500. Also, there is an additional conventional hydrogen bond attraction with the nitrogen atom in the benzene ring to SER 568 residue (Fig. 4). Cromolyn has two additional distinctive, attractive charge interactions through the Zn^{2+} ion and HIS 610. Additionally, π -alkyl interactions with PRO 501 and LEU 749, conventional hydrogen bonding with SER 568 and π - π stacked and π - π T-shaped interactions with the crucial amino acid residues HIS 500, HIS 651, PHE620, and PHE 680 (Fig. 5). Fig. 6. Shows (A) 3D representations of the interactions between HDAC6 and the hit compound ZINC000103531486. (B) The types of nonbonded interactions are indicated in the 2D scheme in respective colors. Various van der Waals, π -sigma interactions with the ALA744, and π -alkyl interaction with PRO501 make compound ZINC000103531486 one

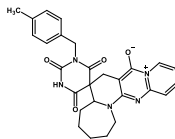
Table 3

The binding energy and inhibition constant values of the hit compounds (structures at the bottom of the table) against HDAC6 and HDAC10 enzymes were calculated using AutoDock 4.2.

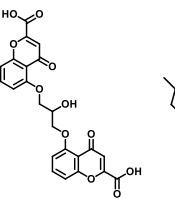
Compound Name	HDAC6		HDAC10		Selectivity
	ΔG (kcal/mol)	Ki (nM)	ΔG (kcal/mol)	Ki (nM)	
Belinostat (Reference)	-9.44	119.44	-6.75	11136	HDAC6
BDH 33926500	-12.70	0.48	-9.73	72.43	HDAC6
CID 667061	-11.10	7.15	-8.80	348.67	HDAC6
Cromolyn	-10.96	9.06	-6.84	9565	HDAC6
ZINC000103531486	-14.21	0.04	-10.07	40.78	HDAC6



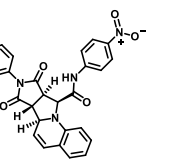
BDH 33926500



CID 667061



Cromolyn



ZINC000103531486

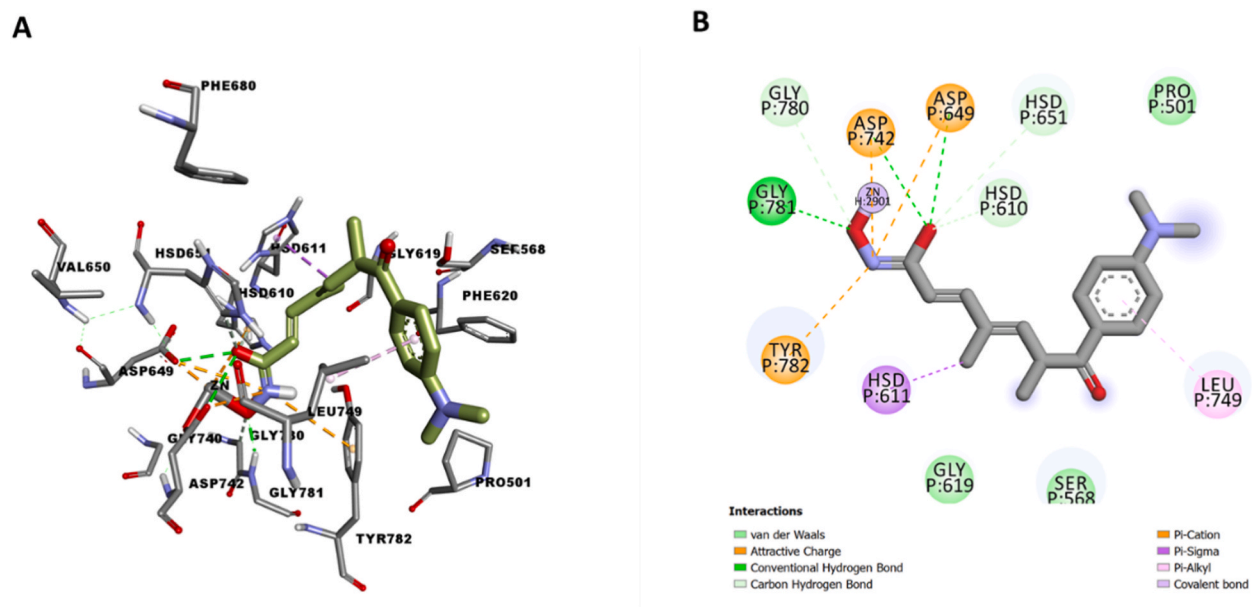


Fig. 2. (A) 3D representations of the interactions between HDAC6 and Trichostatin A (TSN). (B) The types of nonbonded interactions are indicated in the 2D scheme in respective colors.

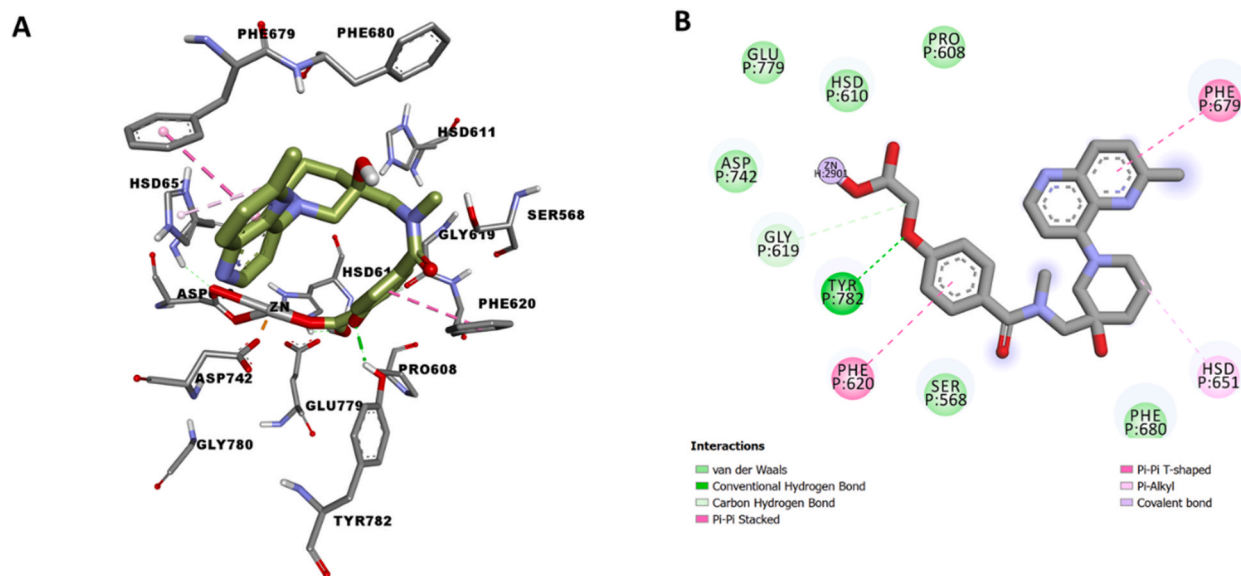


Fig. 3. (A) 3D representations of the interactions between HDAC6 and the hit compound BDH33926500. (B) The nonbonded interactions are shown in the 2D scheme as respective colors.

of the best inhibitors.

3.3. Molecular dynamics simulation analysis

M.D. simulation has proven effective in examining the stability of ligand binding mode [25]. Ideally, the ligand should remain bound to the protein even though conformational adjustment can occur [26]. We superimposed the docking and M.D. simulation poses obtained during the last ten ns. The ligands do not undergo a significant conformational adjustment (Fig. 7). Nonetheless, CID667061, Cromolyn, and ZINC000103531486 show adjustment of the capping groups at the entrance to the enzymes' active site with respective RMSD values of 1.94, 1.98, and 1.9 Å. Therefore, to get a sense of the overall system behavior, measures of structural stability which include RMSD, RMSF, and Rg profiles were analyzed (Fig. 8).

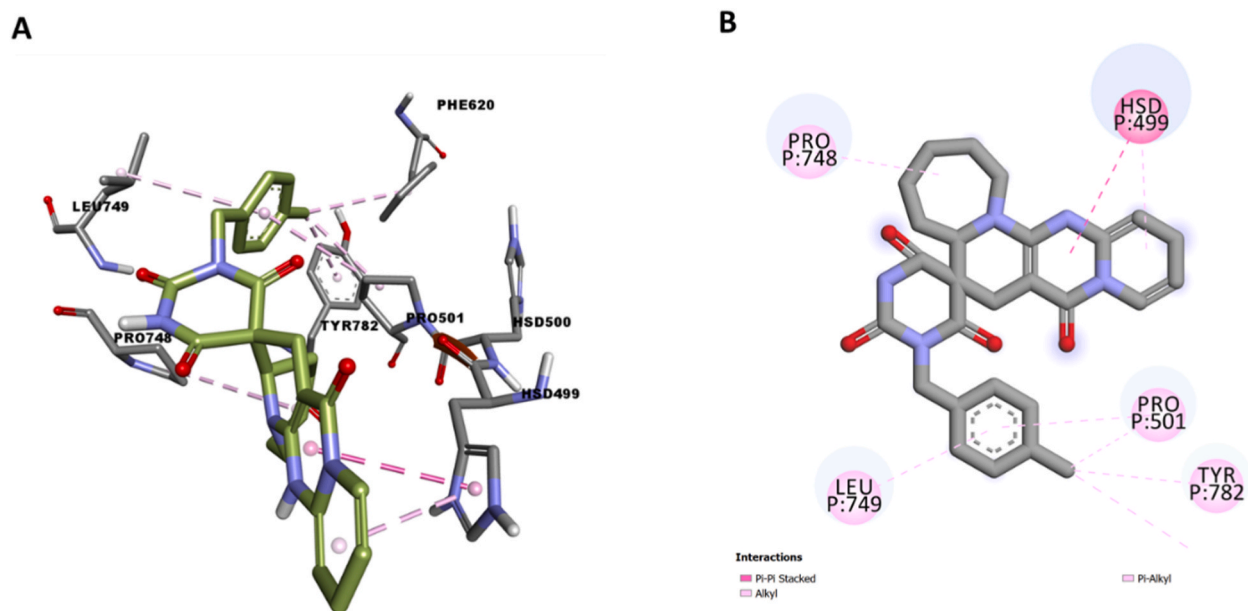


Fig. 4. (A) 3D representations of the interactions between HDAC6 and the hit compound CID667061. (B) The types of nonbonded interactions are indicated in the 2D scheme in respective colors.

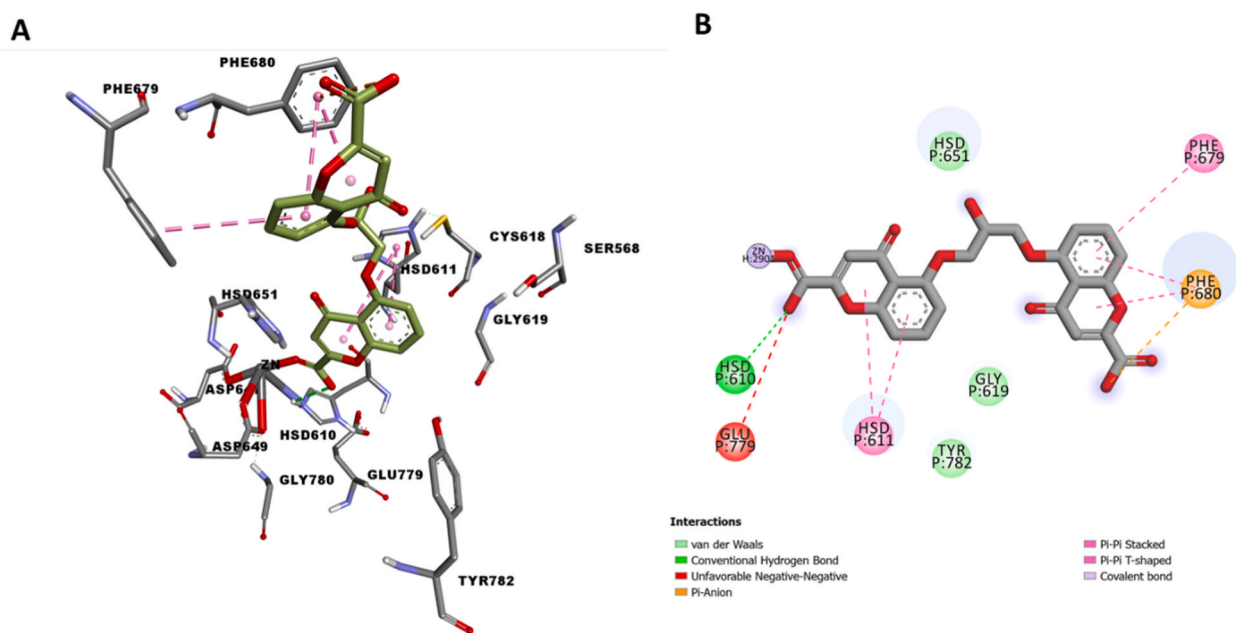


Fig. 5. (A) 3D representations of the interactions between HDAC6 and the hit compound Cromolyn. (B) The types of nonbonded interactions are indicated in the 2D scheme in respective colors.

3.3.1. Root mean square deviation (RMSD) analysis

The root-mean-squared deviation (RMSD) measures the average distance between the atoms of superimposed proteins. RMSD assesses protein structural stability [27]. RMSD plots of the free HDAC6 enzyme, HDAC6 with TSN, and its complex systems with BDH33926500, CID667061, Cromolyn, and ZINC000103531486 are shown in Fig. 8(A). All the studied systems offer a stable state throughout the M.D. simulations. The RMSD of the free HDAC6 enzyme and its known inhibitor TSN slowly and steadily increases from ~ 2 Å to ~ 3 Å and then stabilizes through the simulation. The RMSD of the HDAC6_BDH33926500 complex rises from ~ 1.5 Å to ~ 2.8 Å and then converges toward the end of the simulation. The HDAC6_CID667061 complex shows a steady RMSD profile for the first 40

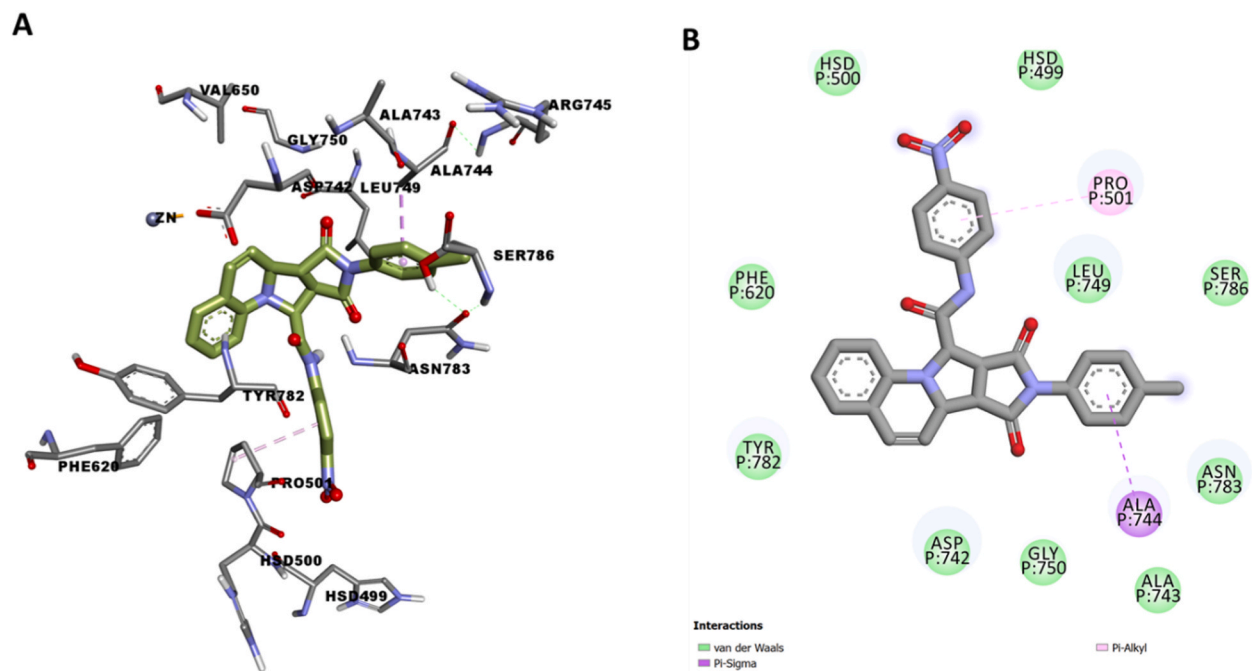


Fig. 6. (A) 3D representations of the interactions between HDAC6 and the hit compound ZINC000103531486. (B) The types of nonbonded interactions are indicated in the 2D scheme in respective colors.

ns, with an RMSD average of 2 Å to 2.8 Å, then increases to ~3.2 Å between 50 and 70 ns and gradually decreases to around 2.5 Å in 85 ns. Afterward, the system slowly increases again and finally stabilizes with an average RMSD of ~2.8 Å after 90 ns of the simulation. The HDAC6_Cromolyn complex shows a stable increase in the RMSD profile (between 1.8 and 3 Å) and converges over time. Similarly, the HDAC6_ZINC000103531486 complex shows a steady RMSD profile ranging from 1.5 Å to 3 Å.

3.4. Root mean square fluctuation (RMSF) analysis

The root-mean-squared fluctuation (RMSF) profiles of the simulated systems of HDAC6 are shown in Fig. 8(B). RMSF shows local residual fluctuation, which directly correlates with the system's stability [28]. HDAC6_BDH33926500 complex system shows a lower RMSF profile compared to the system. In the HDAC6_BDH33926500 complex, GLY 203, PRO 268, and LEU 326 amino acid residues are in the loop region and thus show high fluctuation. In the HDAC6_CID667061 complex, ASP 204 and PRO 201, also in the loop region, display relatively lower amino acid residue fluctuations of the protein than the other complex systems. HDAC6_Cromolyn complex demonstrates amino acid fluctuations in the residues LEU 15, ASP 204, PRO 268, and LEU 326, as they occupy highly flexible loop regions. On the other hand, residues interacting with the ligand atoms do not fluctuate high through the simulation. Cromolyn is structurally similar to Quercetin, a naturally occurring phytochemical with HDAC inhibitory activity [29].

3.5. The radius of gyration (Rg) analysis

The radius of gyration (Rg) measures protein compactness, reflecting stability [30]. The Rg profiles of the free HDAC6 and its complexes with the four hits are plotted in Fig. 8(C). All the systems show low Rg trends (<2.00 Å) over 100 ns.

4. Conclusion

This study conducted an elaborate virtual screening of multiple compound libraries to identify potential selective inhibitors of HDAC6, an isoform implicated in the progression of diverse cancers. Four compounds (BDH33926500, CID667061, Cromolyn, and ZINC000103531486) show potential selectivity for HDAC6 over HDAC10, the structurally related isoform. Furthermore, these compounds bind to HDAC6 with traditional pharmacophore features: Capping group, linker, and zinc-binding domain. They also show good ADMET properties. Therefore, we propose them as potential HDAC6-selective inhibitors to serve as scaffolds for further optimization.

Data availability

All data created or examined in this work are included in this article.

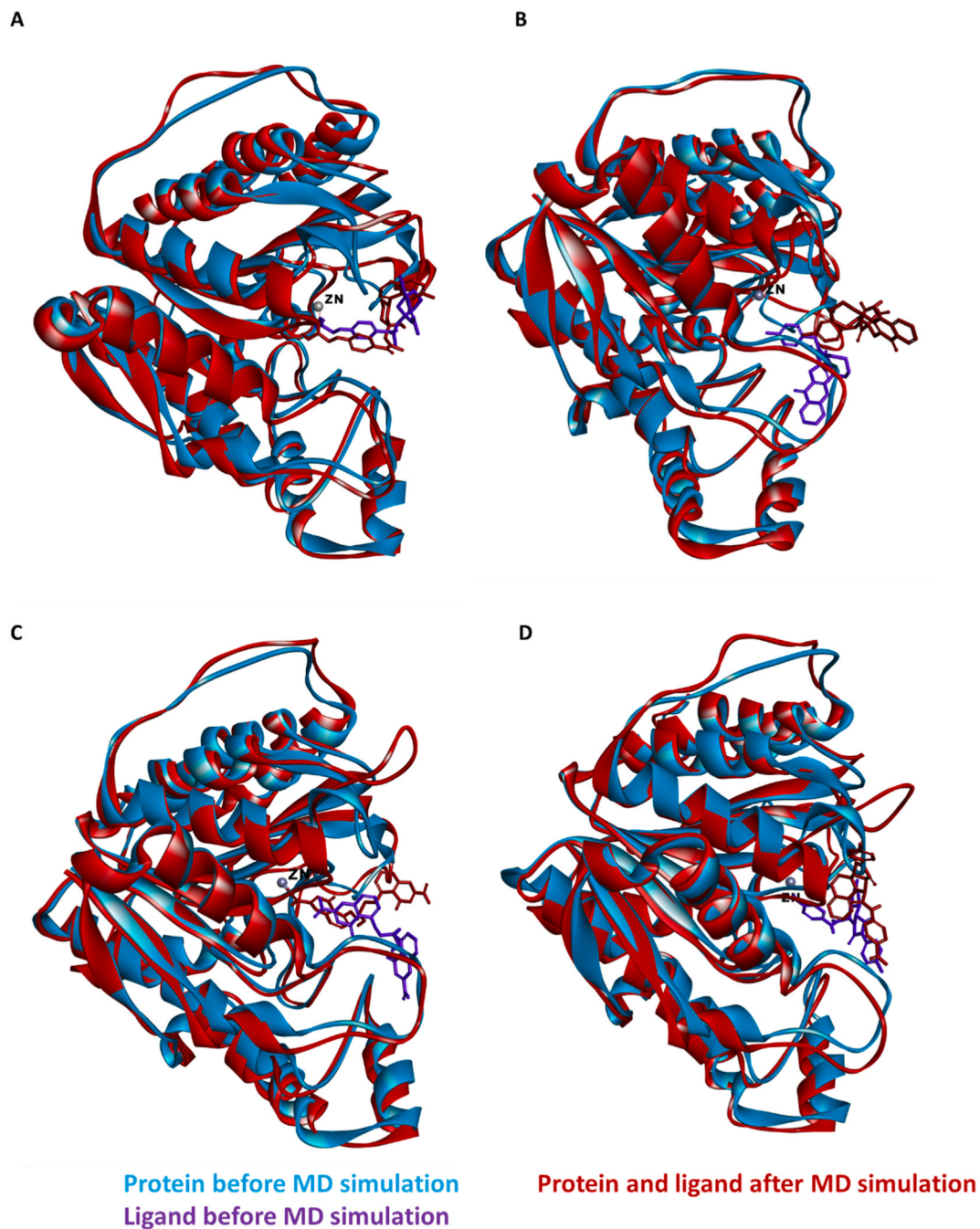


Fig. 7. Superimposition of the top hit compounds' docking and M.D. simulation poses (BDH33926500, CID667061, Cromolyn, and ZINC000103531486).

CRedit authorship contribution statement

Naz Mina Mert: Validation, Data curation. **Buse Erdogan:** Writing – review & editing, Visualization, Software. **Kemal Yelekci:** Writing – review & editing, Writing – original draft, Supervision, Data curation, Conceptualization.

Declaration of competing interest

The authors declare the following financial interests/personal relationships which may be considered as potential competing interests: Kemal Yelekci reports was provided by Kadir Has University. Kemal Yelekci reports financial support was provided by Health

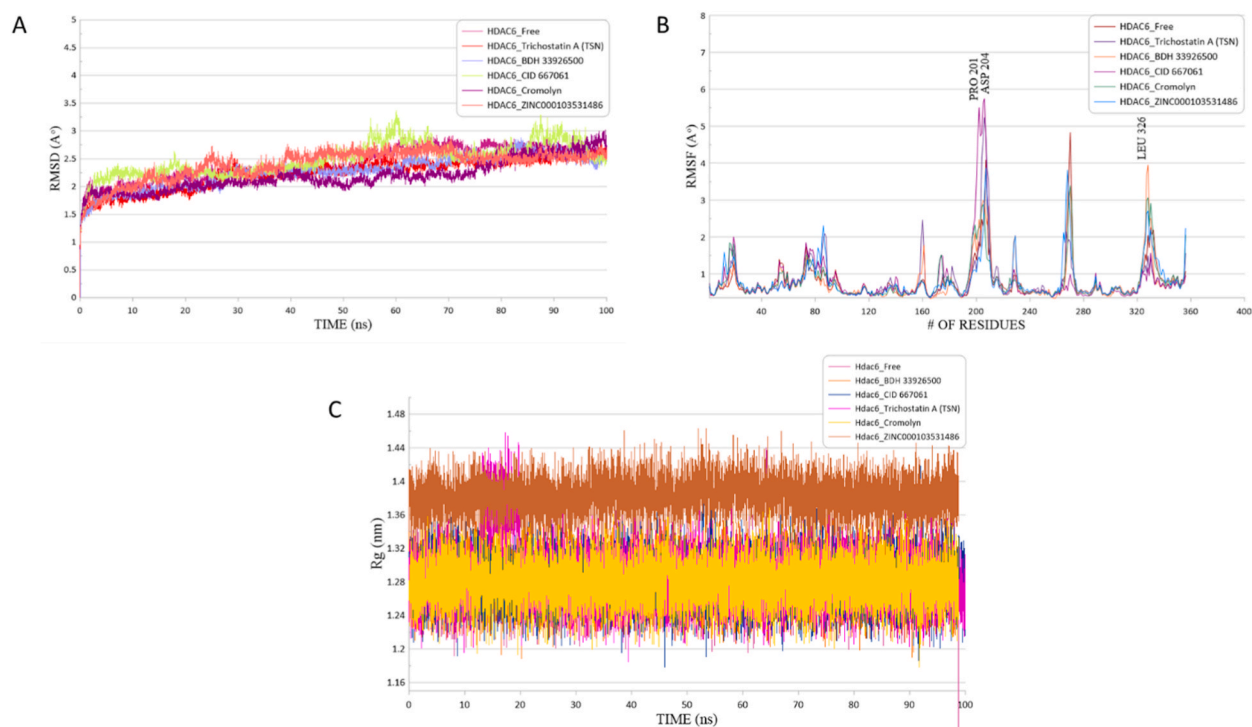


Fig. 8. (A) Root-mean-square displacement (RMSD), (B) root-mean-square fluctuation, and (C) radius of gyration (R_g) profiles computed over 100 ns simulation of the HDAC6 complexes with TSN, BDH33926500, CID667061, Cromolyn, and ZINC000103531486.

Institutes of Türkiye (TUSEB). If there are other authors, they declare that they have no known competing financial interests or personal relationships that could have appeared to influence the work reported in this paper.

Acknowledgment

We thank the Health Institutes of Türkiye (TUSEB) for supporting this research, Project number 4085.

References

- [1] S. Sharma, T.K. Kelly, P.A. Jones, Epigenetics in cancer, *Carcinogenesis* 31 (1) (2009) 27–36, <https://doi.org/10.1093/carcin/bgp220>.
- [2] A. Mai, S. Massa, D. Rotili, I. Cerbara, S. Valente, R. Pezzi, S. Simeoni, R. Ragna, Histone deacetylation in epigenetics: an attractive target for anticancer therapy, *Med. Res. Rev.* 25 (3) (2005) 261–309, <https://doi.org/10.1002/med.20024>.
- [3] L.T. Kagohara, G.L. Stein-O'Brien, D. Kelley, E. Flam, H.C. Wick, L.V. Danilova, H. Easwaran, A.V. Favorov, J. Qian, D.A. Gaykalova, E.J. Fertig, Epigenetic regulation of gene expression in cancer: techniques, resources and analysis, *Briefings in Functional Genomics* 17 (1) (2018) 49–63, <https://doi.org/10.1093/bfpg/elix018>.
- [4] P. Gallinari, S. Di Marco, P. Jones, M. Pallaoro, C. Steinkühler, HDACs, histone deacetylation, and gene transcription: from molecular biology to cancer therapeutics, *Cell Res.* 17 (3) (2007) 195–211, <https://doi.org/10.1038/sj.cr.7310149>.
- [5] Y. Li, E. Seto, HDACs and HDAC inhibitors in cancer development and therapy, *Cold Spring Harbor Perspectives in Medicine* 6 (10) (2016) 1–34, <https://doi.org/10.1101/cshperspect.a026831>.
- [6] J.E. Bradner, N. West, M.L. Grachan, E.F. Greenberg, S.J. Haggarty, T. Warnow, R. Mazitschek, Chemical phylogenetics of histone deacetylases, *Nat. Chem. Biol.* 6 (3) (2010) 238–243, <https://doi.org/10.1038/nchembio.313>.
- [7] D. Wang, *Computational studies on the histone deacetylases and the design of selective histone deacetylase inhibitors* 9 (3) (2009) 241–256.
- [8] A.G. Kazantsev, L.M. Thompson, Therapeutic application of histone deacetylase inhibitors for central nervous system disorders, *Nat. Rev. Drug Discov.* 7 (10) (2008) 854–868, <https://doi.org/10.1038/nrd2681>.
- [9] C. Hubbert, A. Guardiola, R. Shao, Y. Kawaguchi, A. Ito, A. Nixon, M. Yoshida, X.F. Wang, T.P. Yao, HDAC6 is a microtubule-associated deacetylase, *Nature* 417 (6887) (2002) 455–458, <https://doi.org/10.1038/417455a>. 2002 417:6887.
- [10] C. Simões-Pires, V. Zwick, A. Nurisso, E. Schenker, P.A. Carrupt, M. Cuendet, HDAC6 as a target for neurodegenerative diseases: what makes it different from the other HDACs? *Mol. Neurodegener.* 8 (1) (2013) <https://doi.org/10.1186/1750-1326-8-7>.
- [11] K.V. Butler, J. Kalin, C. Brochier, G. Vistoli, B. Langley, A.P. Kozikowski, Rational design and simple chemistry yield a superior, neuroprotective HDAC6 inhibitor, tubastatin A, *J. Am. Chem. Soc.* 132 (31) (2010) 10842–10846, <https://doi.org/10.1021/ja102758v>.
- [12] A.I. Uba, K. Yelekcı, Identification of potential isoform-selective histone deacetylase inhibitors for cancer therapy: a combined approach of structure-based virtual screening, admet prediction and molecular dynamics simulation assay, *J. Biomol. Struct. Dyn.* 36 (12) (2018) 3231–3245, <https://doi.org/10.1080/07391102.2017.1384402>.
- [13] M. Porwal, D. Road, U. Prades, Patients With Relapsed or Refractory Peripheral T-Cell Lymphoma 7 (11) (2016) 4358–4366, [https://doi.org/10.13040/IJPSR.0975-8232.7\(11\).4358-66](https://doi.org/10.13040/IJPSR.0975-8232.7(11).4358-66).
- [14] E.M. Bertino, G.A. Otterson, Romidepsin: a novel histone deacetylase inhibitor for cancer, *Expert Opin. Invest. Drugs* 20 (8) (2011) 1151–1158, <https://doi.org/10.1517/13543784.2011.594437>.

- [15] J.P. Laubach, P. Moreau, J.F. San-Miguel, P.G. Richardson, Panobinostat for the treatment of multiple myeloma, *Clin. Cancer Res.* 21 (21) (2015) 4767–4773, <https://doi.org/10.1158/1078-0432.CCR-15-0530>.
- [16] A.P. Saraswati, N. Relitti, M. Brindisi, J.D. Osko, G. Chemi, S. Federico, A. Grillo, S. Brogi, N.H. McCabe, R.C. Turkington, O. Ibrahim, J. O'Sullivan, S. Lamponi, M. Ghanim, V.P. Kelly, D. Zisterer, R. Amet, P. Hannon Barroeta, F. Vanni, G. Campiani, Spiroindoline-capped selective HDAC6 inhibitors: design, synthesis, structural analysis, and biological evaluation, *ACS Med. Chem. Lett.* 8 (2020), <https://doi.org/10.1021/acsmchemlett.0c00395>.
- [17] G.A. Clawson, Histone deacetylase inhibitors as cancer therapeutics, *Ann. Transl. Med.* 4 (15) (2016) 1–5, <https://doi.org/10.21037/atm.2016.07.22>.
- [18] Y. Hai, D.W. Christianson, Histone deacetylase 6 structure and molecular basis of catalysis and inhibition, *Nat. Chem. Biol.* 12 (9) (2016) 741–747, <https://doi.org/10.1038/nchembio.2134>.
- [19] D.S. Biovia, in: *BIOVIA Discovery Studio 2017 R2: A Comprehensive Predictive Science Application for the Life Sciences*, 2017. San Diego, CA, USA.
- [20] T. Sterling, J.J. Irwin, Zinc 15 - ligand discovery for everyone, *J. Chem. Inf. Model.* 55 (11) (2015) 2324–2337, <https://doi.org/10.1021/acs.jcim.5b00559>.
- [21] O. Trott, A.J. Olson, AutoDock Vina: improving the speed and accuracy of docking with a new scoring function, efficient optimization, and multithreading, *J. Comput. Chem.* 31 (2) (2010) 455–461, <https://doi.org/10.1002/jcc.21334>.
- [22] C.A. Lipinski, Lead- and druglike compounds: the rule-of-five revolution, *Drug Discov. Today Technol.* 1 (4) (2004) 337–341, <https://doi.org/10.1016/j.ddtec.2004.11.007>.
- [23] J.C. Phillips, R. Braun, W. Wang, J. Gumbart, E. Tajkhorshid, E. Villa, C. Chipot, R.D. Skeel, L. Kalé, K. Schulten, Scalable molecular dynamics with NAMD, *J. Comput. Chem.* 26 (16) (2005) 1781–1802, <https://doi.org/10.1002/jcc.20289>.
- [24] J. Lee, X. Cheng, J.M. Swails, M.S. Yeom, P.K. Eastman, J.A. Lemkul, S. Wei, J. Buckner, J.C. Jeong, Y. Qi, S. Jo, V.S. Pande, D.A. Case, C.L. Brooks, A. D. MacKerell, J.B. Klauda, W. Im, CHARMM-GUI input generator for NAMD, GROMACS, AMBER, OpenMM, and CHARMM/OpenMM simulations using the CHARMM36 additive force field, *J. Chem. Theor. Comput.* 12 (1) (2016) 405–413, <https://doi.org/10.1021/acs.jctc.5b00935>.
- [25] S.A. Hollingsworth, R.O. Dror, Molecular dynamics simulation for all, *Neuron* 99 (6) (2018) 1129–1143, <https://doi.org/10.1016/j.neuron.2018.08.011>.
- [26] M. Kovermann, C. Grundström, A. Elisabeth Sauer-Eriksson, U.H. Sauer, M. Wolf-Watz, Structural basis for ligand binding to an enzyme by a conformational selection pathway, *Proc. Natl. Acad. Sci. U.S.A.* 114 (24) (2017) 6298–6303, <https://doi.org/10.1073/pnas.1700919114>.
- [27] A. Kuzmanic, B. Zagrovic, Determination of ensemble-average pairwise root mean-square deviation from experimental B-factors, *Biophys. J.* 98 (5) (2010) 861–871, <https://doi.org/10.1016/j.bpj.2009.11.011>.
- [28] L. Martínez, Automatic identification of mobile and rigid substructures in molecular dynamics simulations and fractional structural fluctuation analysis, *PLoS One* 10 (3) (2015) 1–10, <https://doi.org/10.1371/journal.pone.0119264>.
- [29] B. Salehi, L. Machin, L. Monzote, J. Sharifi-Rad, S.M. Ezzat, M.A. Salem, R.M. Merghany, N.M. El Mahdy, C.S. Killç, O. Sytar, M. Sharifi-Rad, F. Sharopov, N. Martins, M. Martorell, W.C. Cho, Therapeutic potential of Quercetin: new insights and perspectives for human Health, *ACS Omega* 5 (20) (2020) 11849–11872, <https://doi.org/10.1021/acsomega.0c01818>.
- [30] M.T. Khan, A. Khan, A.U. Rehman, Y. Wang, K. Akhtar, S.I. Malik, D.Q. Wei, Structural and free energy landscape of novel mutations in ribosomal protein S1 (rpsA) associated with pyrazinamide resistance, *Sci. Rep.* 9 (1) (2019) 1–12, <https://doi.org/10.1038/s41598-019-44013-9>.